Nuclear Engineering and Technology 52 (2020) 1881–1895

Contents lists available at ScienceDirect

Nuclear Engineering and Technology

journal homepage: www.elsevier.com/locate/net

Original Article

Overcoming the challenges of Monte Carlo depletion: Application to a material-testing reactor with the MCS code

Vutheam Dos, Hyunsuk Lee, Yunki Jo, Matthieu Lemaire, Wonkyeong Kim, Sooyoung Choi, Peng Zhang, Deokjung Lee*

Department of Nuclear Engineering, Ulsan National Institute of Science and Technology, 50 UNIST-gil, Ulsan, 44919, Republic of Korea

ARTICLE INFO

Article history:
Received 5 June 2019
Received in revised form
5 January 2020
Accepted 7 February 2020
Available online 23 February 2020

Keywords:
MCS
Monte Carlo depletion
MCNP6
Material-testing reactor

ABSTRACT

The theoretical aspects behind the reactor depletion capability of the Monte Carlo code MCS developed at the Ulsan National Institute of Science and Technology (UNIST) and practical results of this depletion feature for a Material-Testing Reactor (MTR) with plate-type fuel are described in this paper. A verification of MCS results is first performed against MCNP6 to confirm the suitability of MCS for the criticality and depletion analysis of the MTR. Then, the dependence of the effective neutron multiplication factor to the number of axial and radial depletion cells adopted in the fuel plates is performed with MCS in order to determine the minimum spatial segmentation of the fuel plates. Monte Carlo depletion results with 37,800 depletion cells are provided by MCS within acceptable calculation time and memory usage. The results show that at least 7 axial meshes per fuel plate are required to reach the same precision as the reference calculation whereas no significant differences are observed when modeling 1 or 10 radial meshes per fuel plate. This study demonstrates that MCS can address the need for Monte Carlo codes capable of providing reference solutions to complex reactor depletion problems with refined meshes for fuel management and research reactor applications.

1. Introduction

Since its inception, the Monte Carlo (MC) method has attracted much interest in the field of reactor core analysis due to its multiple advantages over deterministic methods, including flexible geometry modeling with only a limited number of approximations and exact treatment of continuous-energy cross-sections. MC codes can provide reference solutions of the particle transport problem when enough particle histories are simulated, at the downside of important computing time for large-scale reactor problems.

A specific challenge of MC simulation is the reactor depletion simulation, in which transport and depletion steps are successively conducted to simulate one or several reactor cycles. In its most basic form (simple predictor depletion scheme), reaction rates are tallied in each depletion cell during the transport step and are then applied in the depletion step to solve the Bateman equations and update the material compositions. Specific bottlenecks of Monte Carlo codes for depletion simulation are the memory requirement (storage of all the reaction rates and all the material compositions in the depletion solver) and the long simulation time/required CPU power associated with several transport steps which all require preliminary convergence of the fission source distribution before the reaction rates can start being accumulated. Other issues involve the propagation of the statistical uncertainty of the tallied reaction rates on the calculated compositions and desired tally information (neutron multiplication factor, flux, etc.), and a refueling capability to re-use the compositions calculated from a previous cycle for the next cycle.

One topic of interest is the depletion simulation applied to material-testing reactors (MTRs), in which material or fuel samples are irradiated under high values of neutron flux for the purpose of material strength studies or medical radio-isotopes production [1]. Examples of MTRs include the OSIRIS reactor in Saclay, France (shutdown in 2015) [2], the future Jules Horowitz Reactor in Saint-Paul-Lez-Durance, France [3], the Advanced Test Reactor in Idaho National Laboratory, USA [4] or the Jordan Research Training

* Corresponding author. School of Mechanical, Aerospace and Nuclear Engineering, Ulsan National Institute of Science and Technology, 50 UNIST-gil, Ulsan, 44919, Republic of Korea.
E-mail addresses: dosvutheam8@unist.ac.kr (V. Dos), hyunsuklee@unist.ac.kr (H. Lee), yunki.jo@unist.ac.kr (Y. Jo), mlemaire@unist.ac.kr (M. Lemaire), poryor@unist.ac.kr (W. Kim), schoi@unist.ac.kr (S. Choi), zhangpeng@unist.ac.kr (P. Zhang), deokjung@unist.ac.kr (D. Lee).

https://doi.org/10.1016/j.net.2020.02.003

Reactor in Ar Ramtha, Jordan [5]. For such typical plate-fuel-type MTRs, burnup can reach much higher values than in conventional pressurized water reactors (PWRs), in the order of 100 GWd/MTU per assembly or more [6]. A particular emphasis must be put on calculating the axial distribution of burnup in the fuel assemblies with enough axial meshes, as a too low number of axial depletion cells can bias the calculations of neutron flux that are required for MTR performance studies (prediction of neutron flux spectrum, displacements per atom and nuclear heating in irradiated samples). Such bias on the neutron and photon flux in irradiation channels when neglecting the axial burnup distribution has been observed in the OSIRIS MTR [7]. Another crucial point is the accurate determination of the length of MTR operation cycles through depletion calculations. As MTRs can operate for cycles as short as 30 effective full power days (EFPDs) [8], an uncertainty of 1 EFPD on the length of the cycle has a much stronger impact on the fuel consumption and economy of MTRs than for PWRs which present much longer operating cycle (at least one year usually).

The study [7] suggests that the accurate determination of the burnup distribution for plate-fuel-type MTRs requires at least 7 axial depletion cells per fuel plate. For an MTR with 20–40 assemblies containing each about 20 fuel plates, the resulting number of depletion cells may range from ~3,000 to ~6,000 cells. Those numbers of depletion cells can prove too much for an MC code (due to memory and calculation time bottlenecks) and deterministic codes have to be employed instead to provide reference depletion results. An example is the HORUS3D/N neutron calculation tool dedicated to the design and safety studies of the Jules Horowitz reactor. HORUS3D/N contains two reference routes for validation purpose: the reference route for beginning-of-life (time step zero) is performed by the Monte Carlo code TRIPOLI-4.9 but the reference route for core calculations during depletion is assumed by the APOLLO2.8-4 code relying on Method of Characteristics (MOC) calculations [9]. Another common workaround to still try to employ MC codes in depletion simulation is to reduce the number of burnup regions in modeling, the number of burnup steps, and/or the number of nuclides employed in the depletion chain [10]. However, those approximations may negate the good characteristics of the MC method and therefore ultimately lead to a loss of accuracy rather than a gain of accuracy. MC codes featuring depletion capabilities can also suffer from a lack of user-friendliness. One example is the MAT card [11] in MCNP6 depletion simulations, which is used inside the BURN card to set which material numbers are depleted during the simulation. Cells sharing the same material number are depleted together even if they have different locations or volumes. Consequently, for the example of N depletion cells starting with fresh fuel, the fresh fuel material composition must be defined N times in the input using N different material cards for the N cells to be depleted separately. A more user-friendly approach would be to define the fresh fuel composition only once in the input, and to specify in another way that the N cells are to be depleted separately.

We now introduce the Monte Carlo code MCS under development in the Computational Reactor physics and Experiment laboratory (CORE) group of the Ulsan National Institute of Science and Technology (UNIST) [12]. The primary development purpose of MCS is the high-fidelity multi-physics simulation of nuclear reactors within reasonable calculation time and memory usage. Features integrated in MCS for large-scale power reactor analysis include depletion, thermal/hydraulics coupling, fuel performance coupling, equilibrium xenon, on-the-fly neutron cross-section Doppler broadening and critical boron search [13]. This study focuses on the performance and user-friendliness of the MCS depletion capability applied to a realistic MTR computational model based on the Jordan Research and Training Reactor [14,15].

The paper is organized as follows. Section 2 gives a brief overview of MCS features and details the specific methodology used in MCS depletion simulations. The computational model of the investigated MTR is described in section 3 and the suitability of MCS for the criticality and depletion analysis of the MTR is checked in section 4 by comparison against MCNP6 for the effective neutron multiplication factor (k-eff) in depletion and for the following neutronics parameters at beginning of cycle: control rod worth, kinetic parameters, reactivity feedback coefficients, neutron flux in irradiation holes and power peaking factors. In section 5, the sensitivity of the k-eff of the MTR in depletion to the number of axial meshes (1, 7, 10 and 20 axial meshes) and of radial meshes (1, 3 and 10 radial meshes) per fuel plate is studied with MCS to determine the minimum spatial segmentation of the fuel that is required for precise depletion calculations. The reference MCS depletion run contains 37,800 depletion cells, that is, 10 axial meshes, and 10 radial meshes per fuel plate, 21 fuel plates per assembly and 18 assemblies in the MTR core. Section 6 draws out the conclusions and perspectives for future studies.

2. MCS Monte Carlo code

2.1. General features

MCS is a neutron/photon transport MC code developed at the Ulsan National Institute of Science and Technology (UNIST) for criticality and shielding applications, designed and optimized to support large-scale problems in reactor physics. The MCS neutron transport capability has been validated against several benchmarks, notably 279 ICSBEP criticality benchmarks [16], the BEAVRS benchmark [17], and the VENUS-2 and Hoogenboom benchmarks [18]. Specifically, MCS depletion capability has been validated against the BEAVRS benchmark [13,17], VERA benchmark [19], PWR spent fuel pool and storage cask [16] and PWR data from Westinghouse 3-loop and OPR-1000 reactors [20,21]. Examples of MCS applications include the analysis of the prismatic very high-temperature reactor [22], the advanced power reactor 1400 MW electricity (APR-1400) [23] and the long-cycle small modular lead-cooled fast reactor [24].

MCS features a 3D geometry modeling capability through constructive solid geometry based on boundary surfaces. It supports the typical MC concepts of universe and lattice to allow the user to define the repeated geometry features of reactor cores efficiently. The basic neutron physics of MCS is based on the data blocks contained in ACE-format files generated by nuclear data processing systems such as NJOY or RXSP. MCS supports probability tables for unresolved-range cross sections, free-gas treatment, treatment of thermal scattering in a bound target nucleus with S (α,β) data and Doppler broadening rejection correction for neutron up-scattering. The modified power method [25] and the coarse mesh finite difference method [26] are available in MCS to accelerate the fission source convergence in criticality calculations. Advanced features and in-line reactor feedbacks integrated into MCS for multi-physics reactor simulation include depletion, coupling with fuel performance code (FRAPCON) and/or thermo-hydraulic code (TH1D, CTF), on-the-fly neutron cross-section Doppler broadening (OpenW), equilibrium xenon and critical boron concentration search [13].

MCS inputs employ the XML format to natively support freedom in the ordering of keywords and in the use of comments, spaces and blank lines. The MCS output adopts Matlab m-file type format for simplified post-processing. The source code of MCS is written in Fortran 2003. MCS is fully parallelized with Message Passing Interface (MPI) to distribute the calculation load over several nodes and maximize computational performance. For parallel fission

source iteration in criticality mode, MCS employs the parallel fission bank algorithm [27] initially implemented in the OpenMC code. The parallel fission bank algorithm takes advantage of the fact that most of the fission sites produced on one processor during one iteration can be used as source sites on that same processor for the next iteration, thus avoiding unnecessary communication between processors. This good property allows the parallel fission bank algorithm to be faster and to be used effectively with more processors than the traditional master-slave parallel algorithm.

2.2. Depletion methods

The MCS burnup calculation capability is based on an in-built solver to simulate the isotopic changes in material compositions caused by the neutron-induced reactions and spontaneous radioactive decays. The burnup analysis module is turned on by declaring in the input the cells subject to depletion using their material names. MCS users can then specify burnup regions by using either a single "material-wise" or "cell-wise" option. The material-wise option assumes that the cells with the same starting material will be depleted together whereas the cell-wise option assumes that the cells will be depleted separately even if they have the same starting material (no additional user effort is necessary, it is not needed to input one material card per fuel cell to perform cell-wise depletion). After declaring the burnup regions, the thermal power and either time or burnup steps must be declared and other options (choice of depletion scheme, use of equilibrium xenon, etc.) can be input.

MCS performs the burnup calculations by means of the Chebyshev Rational Approximation Method (CRAM) [28] matrix exponential method (MEM) to solve the Bateman equations and calculate the atom densities for the next burnup step. CRAM is usually considered a superior solver to tackle burnup calculation problems because it involves all the nuclides in the core and it can exploit the sparsity of the burnup matrix. CRAM solver is found to be fast and accurate compared to ORIGEN solver and linear chains method solvers [29], and it is found to solve longer burnup intervals more accurately than CINDER90 used in MCNP6 and ORIGEN2 used in MCODE (MCNP5 with ORIGEN2 depletion solver) [30]. The Gauss-Seidel iterative method is used in MCS to accelerate the depletion calculation in the CRAM solver. The CRAM solver takes advantage of MCS parallelization with MPI to provide a robust and accurate solution to the burnup equations with short computation time. To help simulate the continuous change of the reaction rates during each burnup step, semi-predictor corrector and full-predictor corrector (PC) schemes are implemented in MCS in addition to the basic simple predictor scheme. Those two depletion schemes are based on the extrapolation of the nuclide densities at two consecutive time steps during the predictor phase and then, the interpolation of those nuclide densities to obtain the reaction rates applied in the corrector phase. Therefore, those depletion schemes attenuate the negative effects of the constant reaction rate approximation when solving the depletion equations for one burnup step. The burnup chain of MCS can support up to 3,820 nuclides as given in the ENDF decay library, but only 1,373 nuclides are included by default to reduce the computational cost. Those 1,373 nuclides correspond roughly to the nuclides with number densities above 10^{-50} #/barn-cm during standard PWR depletion simulations (the user can increase the number of nuclides included in the burnup chain directly in MCS input for one's needs). All the transmutation paths by radioactive decay present in the evaluated data library are explicitly considered for all the 1,373 nuclides, i.e. beta decay, electron capture, alpha decay, etc. Seven major types of reactions are considered for the modeling of neutron-induced transmutations: (n, absorption), (n,f), (n,γ), (n,2n), (n,3n), (n,α) and (n,p). The corresponding reaction rates are only tallied for the nuclides with available neutron-transport cross sections (that is, 393 nuclides in the ENDF/B-VII.0 library) and with number densities above 10^{-13} #/barn-cm during depletion [31]. For the MTR depletion calculations presented in this paper, 251 nuclides satisfy those two conditions.

Two important points for the efficiency of Monte Carlo depletion is the tally efficiency (to tally all the required reaction rates in all the depletion cells) and the memory use (to store all the depletion-related variables). We address those two points specifically for MCS.

To increase the tally efficiency in MCS when handling large numbers (a few millions or more) tallies, MCS employs a hash function and an indexing array to improve the searching and scoring time of the individual tally bins [32]. The hash function quickly computes the base index of any cell using only the lattice, universe and cell IDs used during the transport simulation. The indexing array is a predefined array which associates the base index of a cell with its corresponding tally bin indices. For instance, the user can define additional indexing systems in the MCS input such as a pin-wise, assembly-wise or material-wise index to be used in depletion calculation and tallies in MCS. In that case, the indexing array will associate to the base index of each cell three additional indices: the corresponding tally bin indices in the pin-wise, assembly-wise and material-wise indexing systems respectively. This hash indexing algorithm has proven to be efficient and robust for MCS PWR simulations, with a tally bin searching overhead of less than 1% up to 10 million tally bins [12].

Large memory is required to store the burnup information on each processor for large-scale problems (a few hundred thousand depletion cells or more), usually exceeding the available memory on most clusters [33]. In MCS, the burnup-related information which needs to be stored for one single depletion cell are: the material variables for transport, the reaction rates for scoring (3-group fission, absorption, (n,γ), (n,2n), (n,3n), (n,α), (n,p)), the reaction rates for statistical process and the number densities used in the CRAM solver. For MTR depletion, the memory use for one depletion cell where the number densities of 1,373 nuclides are tracked and the reactions rates of 251 nuclides are tallied is estimated as below:

- M1 (material variables for transport): 6,204 bytes = 251 nuclides x 2 densities (gram and isotopic) x 8 bytes +251 nuclides x 2 pointers (ZA and cross-section) x 4 bytes
- M2 (reaction rates for scoring): 18,072 bytes = 251 nuclides x 9 reaction rates x 8 bytes
- M3 (reaction rates for the statistical process): 34,144 bytes = 251 nuclides x 9 reaction rates x 2 scores (sum and sum^2) x 8 bytes
- M4 (number densities for the CRAM solver): 21,968 bytes = 1,373 depletion chain nuclides x 2 densities (predictor and corrector step) x 8 bytes

One important feature is that the memory use M3 and M4 are not required to be duplicated on all the available processors: only saving this information on one processor is enough. This allows the memory use per processor of MCS during depletion calculations to be expressed as in Equation (1):

$$M_{burnup} = \left(M_{all} + \frac{M_{one}}{NP} \right) \times N_c \tag{1}$$

where M_{all} = M1 + M2, M_{one} = M3 + M4, NP is the number of processors and Nc is the number of depletion cells. This feature is implemented in MCS and enables to decrease the memory use per processor for increasing numbers of processors. For 20 processors

and 500,000 depletion cells, the memory use per processor for the depletion process reaches about 13.5 GB.

3. Description of the material-testing reactor model

A plate-fuel-type MTR model is developed for MCS and MCNP6 based on the technical data available in Refs. [14,15,34–36]. The MTR is a 5 MW thermal power open-pool-type nuclear research reactor, located inside the campus of the Jordan University of Science and Technology in Jordan, for the purpose of basic nuclear research, fuel and material testing, training and education in science and engineering as well as medical radioisotope production. The MTR achieved first criticality on April 25, 2016 [35]. The MTR start-up core is composed of fuel assemblies with uranium densities in the range 1.9~4.8 gU/cm^3 whereas its equilibrium core is composed only of fuel assemblies of uranium density 4.8 gU/cm^3.

The summary of important parameters of the MTR is given in Table 1. The MTR core is composed of 18 rectangular fuel assemblies (FA) in grid pattern with 21 fuel plates per assembly. The fuel consists of uranium silicide in an aluminum matrix (U_3Si_2–Al) in the form of a thin sheet referred to as the fuel "meat". Each fuel assembly is composed of 21 fuel meats (62.1 mm long, 0.51 mm thickness, and 640 mm height) with density of 6.5 g/cm^3. Each fuel meat is surrounded by fuel plates of aluminum cladding. A group of 21 plates with 1.27 mm thickness are held together by metal side-plates, with space for coolant flow between adjacent plates, constituting a rectangular fuel assembly. A schematic of a plate fuel assembly is shown in Fig. 1(left). The outer dimensions are 77.2 mm by 77.2 mm horizontally with 996 mm vertical height. Four square-ring control absorber rods (CARs) made of hafnium, shown in Fig. 1(right, yellow part), can be inserted from top to bottom around the assemblies FA05, FA07, FA12 and FA14. They are used to maintain the core neutron population at the desired level and also serve as a safety rod. Two second shutdown rods (SSRs) made of boron carbide (B_4C) are also used to shut down the reactor.

The MTR is cooled and moderated by light water which flows upwards through the core. A cylindrical tank of heavy water of 1.5 m radius and 3.0 m height surrounds the core and is itself surrounded by an even bigger pool of light water. In the heavy water reflector region, the irradiation holes are filled with light water or plugged with aluminum. The experimental facilities around the MTR core include two standard beam tubes (ST1 and ST2), a cold neutron source beam tube (CN), a neutron radiography beam tube (NR) and a thermal neutron column (TH). The cold neutron source beam tube is filled with helium and the thermal neutron column is made from graphite.

Table 1
Materials and dimensions of the MTR core.

Parameters	Description
Coolant and moderator	Light water
Reflector	D_2O, Be
Clad material	Aluminum
Fuel material	U_3Si_2–Al
Fuel meat density (g/cm^3)	6.5
Whole core dimensions (mm)	3000 x 3000 x 3000
CAR dimensions (mm)	97.2 x 97.2 x 966
Number of fuel assemblies	18
Fuel assembly dimensions (mm)	77.2 x77.2 x 966
Fuel meat thickness (mm)	0.51
Cladding thickness (mm)	0.38
Fuel plate thickness (mm)	1.27
Fuel plate length (mm)	680
Fuel plate width (mm)	66.6
Coolant channel thickness (mm)	2.35
Number of fuel plates per assembly	21

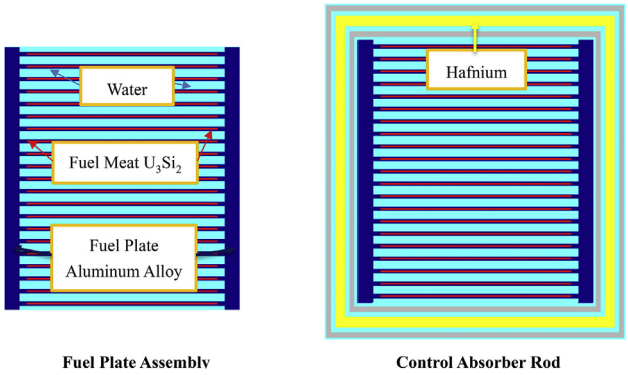

Fig. 1. Top view of fuel plate assembly and hafnium control absorber rod.

The core configuration of the MTR modeled in MCS and based on the MTR is shown in Fig. 2. The black dotted line on the core top view (left-hand side) shows the location of the cut for the core side view (right-hand side). The adopted FA loading pattern is shown in Fig. 3, with four groups of FAs having different uranium enrichments: 7.5 wt %, 10.5 wt %, 16 wt %, and 19.75 wt %. A flux trap is modeled in the irradiation hole at the center of the core with an irradiation ring (IR), which is an aluminum dummy ring filled with beryllium. All the other irradiation holes are filled with beryllium except for the locations IR12 and IR14, which are filled with samples made of tellurium oxide (TeO_2) and manganese oxide (MnO_3) respectively. The whole core geometry of the MTR modeled in MCS is shown in Fig. 4.

4. Criticality and depletion analysis of the material-testing reactor

The suitability of MCS for the criticality and depletion analysis of the MTR is first verified by comparison of MCS results against MCNP6 results for the following parameters at beginning of cycle (BOC): control absorber rod worth, kinetic parameters, reactivity feedback coefficients, neutron flux in irradiation holes and power peaking factors; and for the k-eff in depletion. For all the calculations, the cross-section, fission yield, and radioactive decay data are based on the ENDF/B-VII.0 evaluated nuclear data library processed by NJOY at a single temperature (in this case room temperature). To account for the chemical binding effects in the scattering of thermal neutrons by light water, heavy water, beryllium and graphite, appropriate thermal scattering libraries based on ENDF/B-VII.0 are used in the calculations.

4.1. Control absorber rod worth

The integral and differential rod worth of the four CARs of the MTR are determined at BOC. The integral rod worth is calculated based on the reactivity change between the two states when the four control rods are all fully inserted and when they are all partially inserted at a given height. The differential worth determines by how much the reactivity increases when the four CARs are all withdrawn by 1 mm from a given height [37].

For this study, the two SSRs are set to be totally withdrawn. The four CARs are withdrawn together from the bottom of the core (full insertion, height = 0 mm) until they are fully withdrawn (height = 650 mm), the active fuel region ranging from height 10 mm–650 mm. The withdrawal process is conducted in 14 steps, and at each step, the four CARs are moved up by 50 mm. Each criticality calculation is performed with 25 inactive cycles, 400 active cycles and 100,000 neutrons per cycle to achieve low relative statistical uncertainty on the calculated k-eff. The variations of cell-

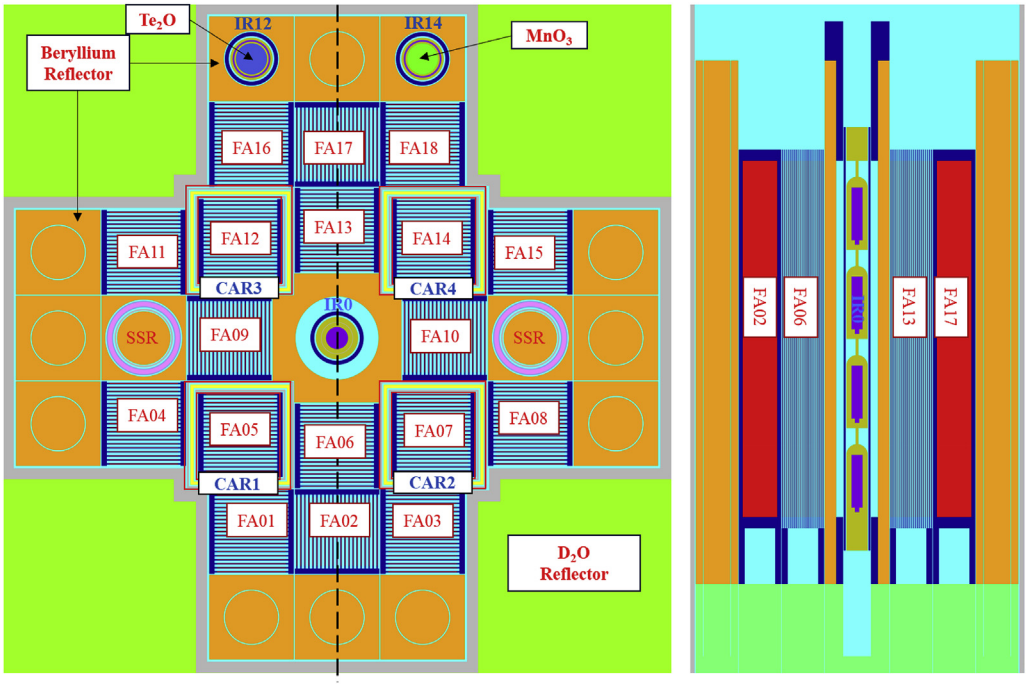

Fig. 2. Core configuration of the modeled fuel-plate-type MTR: top view (left) and side view (right).

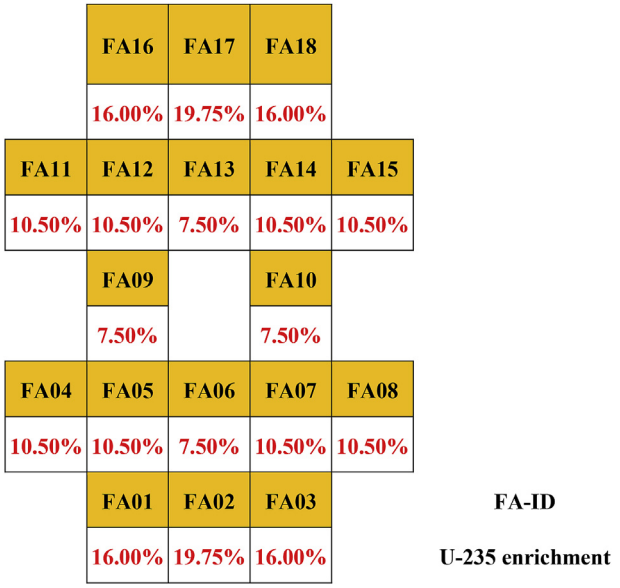

Fig. 3. Loading pattern with different uranium enrichments.

based Shannon entropy and of the center of mass of the fission sources are used to determine that 25 inactive cycles are sufficient for the convergence of the fission source distribution. The k-eff results for each position of the CARs are shown in Table 2 and a good agreement within 3 standard deviations is observed between MCS and MCNP6.

The integral reactivity worth of CARs is calculated as in Eq. (2) and the differential reactivity worth of CARs is calculated as in Eq. (3):

$$I = \rho_i - \rho_0, \tag{2}$$

$$D = \frac{I_{i+1} - I_i}{h_{i+1} - h_i}, \tag{3}$$

where ρ_i is the reactivity for CARs inserted at position h_i, ρ_0 is the reactivity for fully inserted CARs (height $h_0 = 0$ mm) and h_i is the height of the CARs from 0 to 650 mm.

A good agreement between MCS and MCNP6 on the integral worth of CARs versus the height of the CARs can be visualized in Fig. 5 Comparison of integral rod worth of CARs. The relative differences in the calculated integral worth of CARs are less than 1.4% while the total worth of CARs reaches almost 40,000 pcm. The slope of the integral CAR worth curve is greatest when the CARs are at a height of 150 mm.

A good agreement between MCS and MCNP6 on the differential worth of CARs versus the height of the CARs can be observed in Fig. 6 Comparison of differential rod worth of CARs. The relative differences on the calculated differential worth of the CARs range from −6% to 3.2% for the calculation, Consistently with Fig. 5 Comparison of integral rod worth of CARs., the differential CARs worth is the greatest when CARs approach the height of 150 mm.

4.2. Kinetic parameters

The adjoint-weight kinetic-parameter calculation module of MCS [38] is employed to determine the kinetic parameters (effective delayed neutron fraction β_{eff} and mean neutron generation time Λ) of the MTR at BOC. For this calculation, the two SSRs are totally withdrawn, the CARs are set at a height of 350 mm from the bottom, 25 inactive cycles and 400 active cycles with 100,000 neutrons per cycle are used. The kinetic parameters calculated by MCS and MCNP6 are shown in Table 3 with deviations. The results show good agreement with no significant difference between MCS and MCNP6.

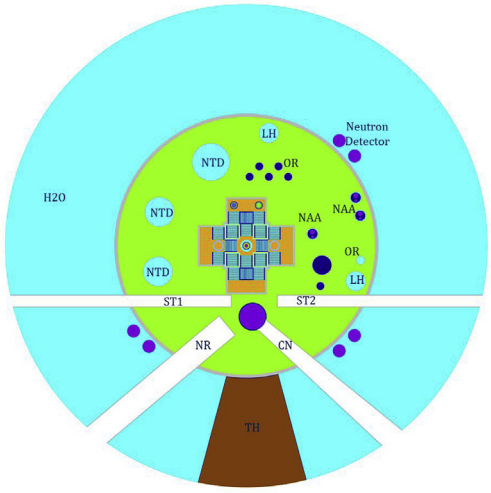

FA: Fuel Assembly

CAR: Control Absorber Rod

SSR: Second Shutdown Rod

IR0: Central Flux Trap

IR1~14: Irradiation Holes

NTD: Neutron Transmutation Doping

LH: Large Irradiation Hole

OR: Outer Region irradiation holes

Fig. 4. Full top view of the modeled fuel-plate-type MTR.

Table 2
Calculated k-eff values with CARs movement from bottom to top.

Altitude (mm)	k-eff ± uncertainty (pcm)		Diff ± 1σ (pcm)
	MCS	MCNP6	
0	0.75608 ± 13	0.75638 ± 12	−30 ± 17
50	0.76798 ± 13	0.76802 ± 12	−4 ± 18
100	0.80106 ± 14	0.80104 ± 11	2 ± 18
150	0.84994 ± 13	0.85035 ± 12	−41 ± 18
200	0.89942 ± 12	0.89914 ± 12	28 ± 17
250	0.94069 ± 13	0.94065 ± 13	4 ± 18
300	0.97515 ± 12	0.97522 ± 13	−7 ± 18
350	1.00309 ± 14	1.00297 ± 13	12 ± 19
400	1.02573 ± 13	1.02570 ± 12	3 ± 17
450	1.04391 ± 13	1.04401 ± 11	−10 ± 17
500	1.05850 ± 13	1.05867 ± 12	−17 ± 18
550	1.06983 ± 12	1.06965 ± 12	18 ± 17
600	1.07756 ± 12	1.07740 ± 12	16 ± 17
650	1.08195 ± 12	1.08207 ± 12	−12 ± 17

*$Diff = 10^5 \times (k_{MCS} - k_{MCNP6})$

4.3. Reactivity feedback coefficient

The calculation of the fuel temperature coefficient α_{FTC}, respectively the moderator temperature coefficient α_{MTC} is done by dividing the variation of reactivity by the corresponding variation of temperature in fuel δT_F or moderator δT_M according to Eq. (4):

$$\alpha_{FTC} = \frac{\delta\rho_F}{\delta T_F} \text{ and } \alpha_{MTC} = \frac{\delta\rho_M}{\delta T_M}. \quad (4)$$

The reactivity change δρ is determined as in Eq. (5):

$$\delta\rho = \frac{k_2 - k_1}{k_2 k_1}, \quad (5)$$

where k_1 and k_2 are respectively the effective neutron multiplication factors for reactor state 1 (fuel temperature T_F or moderator temperature T_M) and state 2 (fuel temperature $T_F + \delta T_F$ or moderator temperature $T_M + \delta T_M$). These temperature reactivity coefficients are calculated between 350K and 400K at BOC with 25 inactive cycles, 400 active cycles and 5 million neutron histories per cycle. All four CARs are inserted at height 350 mm from the bottom of the core. The ENDF/B-VII.0 libraries preprocessed as ACE files at the temperatures 350 K and 400 K are used for fuel and moderator materials. The results reported in Table 4 show good agreement of the temperature coefficient calculations between MCS and MCNP6. The FTC and MTC values are negative, thus ensuring negative reactivity feedback in the event of a power excursion.

4.4. Neutron flux distribution

The neutron flux is calculated for three irradiation holes at BOC. The central irradiation hole IR0 contains four capsules

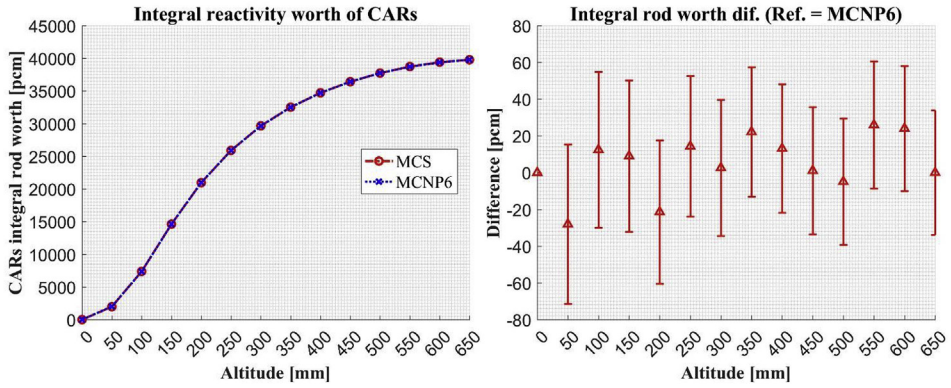

Fig. 5. Comparison of integral rod worth of CARs.

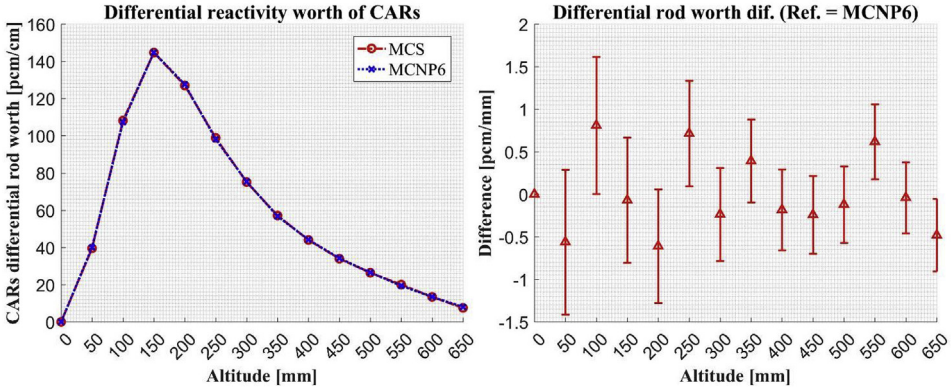

Fig. 6. Comparison of differential rod worth of CARs.

Table 3
Comparison of β_{eff} and Λ results in MCS and MCNP6.

Parameters	MCS	MCNP6
Λ (μs)	123.32 ± 0.6	123.35 ± 0.6
β_{eff} (pcm)	723 ± 16	733 ± 15

stacked on each other axially, with helium filling the center of each capsule. The neutron flux is calculated at the center of each capsule, in helium material. In the peripheral irradiation hole IR12, the neutron flux is calculated in one of the tellurium oxide (TeO_2) sample and the surrounding helium gas. Similarly, in the peripheral irradiation hole IR14, the neutron flux is calculated in one of the manganese oxide (MoO_3) sample and the surrounding helium gas. The top view and the side view of each irradiation hole are shown in Fig. 7. The flux tally results for one neutron source are normalized to 5 MW reactor power using the scaling methodology presented in Ref. [39]. The neutron flux calculated by MCS and MCNP6 in irradiation holes IR0, IR12 and IR14 are reported in Table 5, with relative uncertainties at one standard deviations. Thermal flux indicates neutrons with energies from 0 to 0.625 eV and fast flux corresponds to neutron energies larger than 1 MeV. Good agreement is observed between MCS and MCNP6. The calculation of flux distributions of the irradiation holes in core region shows good consistency with the design purpose of a MTR, that is, to have high flux in the range of 1×10^{13} to 1×10^{14} n/cm^2-s in the core region [14].

4.5. Power peaking factor

We define the total power peaking F_q of an assembly as the ratio of its highest local power density to the average power density in the core:

$$F_q = \frac{Highest\ Local\ Power\ Density}{Average\ Power\ Density\ of\ Core}, \tag{8}$$

and the radial power peaking factor F_r as the power ratio of an assembly, expressed as:

$$F_r = \frac{Power\ Generated\ by\ an\ Assembly}{Average\ Power\ of\ all\ Assemblies}. \tag{9}$$

The peaking factors are calculated at BOC with all control rods fully withdrawn from the core. Each fuel assembly is axially divided into 10 equal segments and the fission power (MCNP6 F7 tally) is then calculated in the 10 axial segments for all the assemblies. The results of F_q and F_r for MCS and MCNP6 are shown in Fig. 8. The results of both codes are consistent and satisfy the usual design requirement that the F_q value should not exceed 3.0 [14].

4.6. Material-wise/assembly-wise depletion

The depletion capability of MCS is verified on two depletion problems against MCNP6. The two depletion problems are made simple enough that they can be run within reasonable calculation time and memory use with the MCNP6 code. The first simple depletion problem is a material-wise depletion where fuel cells with the same initial uranium enrichment are depleted together. There are 4 fuel materials corresponding to 4 different initial values of uranium enrichment in the loading pattern of Fig. 3, and so this first problem only contains 4 depletion cells. The second problem is an assembly-wise depletion where the fuel cells inside one assembly are depleted together. The MTR contains 18 assemblies so this second problem contains 18 depletion cells. Fig. 9 illustrates the material-wise and assembly-wise depletion patterns for the MTR core.

Table 4
Effect of temperature variation on reactivity in MTR.

Temperature coefficient		MCS	MCNP6	Relative Diff* (%) ± 1σ
Fuel	k-eff at 350 K ± 1σ (pcm)	1.00180 ± 2	1.00181 ± 2	
	k-eff at 400K ± 1σ (pcm)	1.00065 ± 2	1.00061 ± 2	
	α_{FTC} [pcm/K] ± 1σ (pcm/K)	−2.29 ± 0.06	−2.39 ± 0.06	−4.17 ± 3.26
Moderator	k-eff at 350 K 1σ (pcm)	0.99707 ± 2	0.99708 ± 2	
	k-eff at 400 K1σ (pcm)	0.98891 ± 2	0.98899 ± 2	
	α_{MTC} [pcm/K]	−16.55 ± 0.06	−16.41 ± 0.06	0.87 ± 0.5

$$Relative\ Diff^* = 100 \times \frac{\alpha_{MCS} - \alpha_{MCNP6}}{\alpha_{MCNP6}}$$

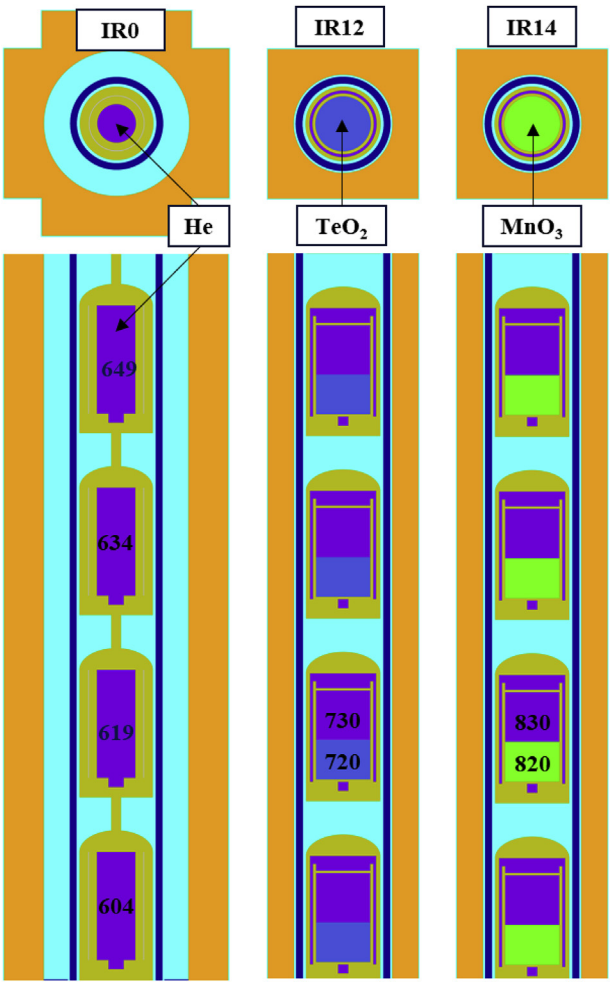

Fig. 7. Top view and side view (on capsule) of calculated irradiation holes.

Each depletion simulation is performed for 100 effective full power days (EPFD) at 5 MW thermal power with 32 time steps. For each transport step, 25 inactive cycles and 175 active cycles are simulated with 50,000 histories per cycle.

The depletion options used in MCNP6 depletion calculations are detailed. MCNP6 employs the full predictor-corrector depletion scheme. The BURN card is used to turn on the depletion calculations. In the BOPT card, the default recoverable energy per fission (Q-value = 1) is used with the Tier 3 fission products. Nuclides with an atom fraction smaller than 1×10^{-10} are excluded. The depletion calculation in MCNP6 is performed with the CINDER90 depletion module using a matrix exponential method (MEM) of similar accuracy with ORIGEN2 depletion solver [30] and tracking about 3600 nuclides [40]. The OMIT card is used to omit 271 specific nuclides from the transport calculations in the MTR core simulation (MCNP6 returns a fatal error and the calculation fails if those 271 nuclides are not omitted). The reaction rates are still generated for the omitted nuclides by matching a 63-group flux calculated by MCNP6 to a 63-group cross section set inherent within CINDER90, yielding 63-group reaction rates integrated with respect to energy to determine the total reaction rates [41]. However, the 63-group cross sections in CINDER90 were collapsed over a generic neutron spectrum that may or may not be representative of the studied MTR and thus it may lead to large discrepancies in the isotope inventory of the daughter products of the concerned reactions [42]. The MCNP6 code only uses material-wise depletion as default and, therefore, as many material cards as depletion cells are defined in the inputs.

The depletion options used in MCS depletion calculations are detailed. The fuel indexing used for burnup calculation is done by referring to the material names as in MCNP6. However, the user is given the possibility for those cells sharing the same materials to specify either a material-wise or cell-wise indexing with the keywords shown in Fig. 10. The semi predictor-corrector depletion algorithm is employed. The concentrations of 1,373 nuclides are tracked in each depletion cell. Fission and transmutation cross-sections are only calculated for the nuclides for which neutron-transport data exist (393 nuclides in ENDF/B-VII.0 library) and for which the number densities are greater than 10^{-13} #/barn-cm. Nuclides with number densities smaller than 10^{-50} #/barn-cm are excluded from the depletion calculation and nuclides with number densities than 10^{-13} #/barn-cm are excluded from the transport calculation. Table 6 sums up the information about the depletion calculations of MCS and MCNP6 for the MTR core.

The memory usage of each code during the depletion calculation is measured with the “top” command on Linux system. The depletion calculations are performed with 40 processes on a Linux cluster with CPUs of type “Intel(R) Xeon(R) CPU E5-2680 v4 @ 2.40 GHz” and 500 GB memory per node. A summary of the execution time and memory usage per CPU for the depletion calculations is presented in Table 7, which shows the good efficiency of MCS overall compared to MCNP6.

The k-eff values at the different time steps of MTR material-wise depletion calculations (4 axially-uniform depletion cells) are presented in Table 8 and can be visualized in Fig. 11 with their statistical uncertainties at one standard deviations. The comparison in Fig. 11 shows similar evolution trends of k-eff over time between MCS and MCNP6 with a maximum k-eff difference of 75 pcm after 0.03 EFPDs, within 3 standard deviations. The cycle length of the MTR is calculated to be about 93 days (this value is expected to be inaccurate because the depletion is axially uniform).

Table 5
Comparison of neutron flux in the irradiation holes.

Irradiation position	Cell No.	Cell material	Thermal flux (10^{13}n/cm^2-s) ± uncertainty (%)			Fast flux (10^{13}n/cm^2-s) ± uncertainty (%)		
			MCS	MCNP6	Diff*(%)	MCS	MCNP6	Diff* (%)
IR0	604	He	2.73 ± 0.5	2.75 ± 0.5	−0.7 ± 0.7	1.16 ± 0.8	1.17 ± 0.8	−0.8 ± 1.1
	619		4.68 ± 0.4	4.66 ± 0.4	0.6 ± 0.6	2.00 ± 0.6	1.98 ± 0.6	1.1 ± 0.9
	634		4.82 ± 0.4	4.80 ± 0.4	0.2 ± 0.5	2.05 ± 0.6	2.05 ± 0.6	0.0 ± 0.8
	649		3.16 ± 0.5	3.18 ± 0.5	−0.6 ± 0.7	1.35 ± 0.7	1.37 ± 0.7	−1.2 ± 1.0
IR12	720	TeO_2	4.79 ± 0.4	4.86 ± 0.5	−1.5 ± 0.7	0.97 ± 1.1	0.96 ± 1.1	0.8 ± 1.6
	730	He	5.64 ± 0.5	5.69 ± 0.5	−0.8 ± 0.6	1.08 ± 0.9	1.04 ± 1.0	3.3 ± 1.3
IR14	820	MnO_3	4.42 ± 0.5	4.42 ± 0.5	0.1 ± 0.7	0.94 ± 1.1	0.92 ± 1.1	2.0 ± 1.6
	830	He	5.53 ± 0.5	5.51 ± 0.5	0.3 ± 0.7	1.07 ± 0.9	1.04 ± 1.0	3.5 ± 1.3

$Diff^* = 100 \times \frac{\varphi_{MCS} - \varphi_{MCNP6}}{\varphi_{MCNP6}}$

	FA16	FA17	FA18	
	1.74	1.54	1.75	
	1.74	1.54	1.74	
	0.12	-0.19	0.65	
FA11	FA12	FA13	FA14	FA15
1.65	1.63	1.48	1.62	1.66
1.67	1.63	1.48	1.63	1.65
-1.55	-0.02	0.25	-0.50	0.57
	FA09		FA10	
	1.48		1.47	
	1.48		1.48	
	-0.20		-0.79	
FA04	FA05	FA06	FA07	FA08
1.69	1.66	1.50	1.64	1.67
1.68	1.67	1.51	1.65	1.67
0.23	-0.65	-0.94	-0.39	0.21
FA ID	FA01	FA02	FA03	
MCS	1.82	1.63	1.80	
MCNP6	1.81	1.62	1.80	
Dif. (%)	0.57	0.20	-0.10	

	FA16	FA17	FA18	
	1.04	1.10	1.03	
	1.04	1.10	1.04	
	-0.20	0.01	-0.32	
FA11	FA12	FA13	FA14	FA15
0.95	1.01	0.86	1.01	0.94
0.95	1.01	0.86	1.01	0.94
-0.26	-0.17	0.16	-0.17	-0.05
	FA09		FA10	
	0.92		0.92	
	0.92		0.92	
	-0.10		0.09	
FA04	FA05	FA06	FA07	FA08
0.96	1.03	0.89	1.03	0.95
0.96	1.03	0.88	1.03	0.94
-0.10	-0.01	0.12	0.06	0.37
FA ID	FA01	FA02	FA03	
MCS	1.11	1.17	1.10	
MCNP6	1.10	1.16	1.09	
Dif. (%)	0.20	0.16	0.20	

Fig. 8. Radial (left) and total (right) power peaking factors for MTR.

Fig. 9. Depletion cells in the MCS model for different depletion modeling options.

```
@ Material-wise depletion fuels index
<indices>
    <name> matwise-fuels </name>
    <material-wise> U3Si2-19.75wt% U3Si2-16.wt% U3Si2-10.5wt% U3Si2-7.5wt% </material-wise>
</indices>

@ Cell-wise depletion fuels index
<indices>
    <name> cellwise-fuels </name>
    <cell-wise> U3Si2-19.75wt% U3Si2-16.wt% U3Si2-10.5wt% U3Si2-7.5wt% </cell-wise>
</indices>
```

Fig. 10. Defining the fuel index for burnup calculation in MCS.

For the assembly-wise depletion (18 axially-uniform depletion cells), the k-eff values at different time steps are shown in Table 9 as calculated by MCS and MCNP6. A good agreement is observed between the two codes, with a maximum k-eff difference of 76 pcm after 2 EFPDs, within 3 standard deviations. The comparison in Fig. 12 shows similar evolution trends of k-eff over time between MCS and MCNP6. The cycle length of the MTR is calculated to be about 92.5 days (this value is expected to be inaccurate because the depletion is axially uniform).

Table 6
MCS and MCNP depletion information for the MTR core.

Code	MCS	MCNP6
Developer	UNIST	LANL
Transport	Monte Carlo	Monte Carlo
Energy Group	Continuous Energy	Continuous Energy
XS Library	ENDF/B-VII.0	ENDF/B-VII.0
Kappa data	SERPENT	MCNP6
Decay Library	ORIGEN2.2	CINDER90
Yield Library	ENDF/B-349	CINDER90
Depletion Solver	MEM (CRAM)	MEM (CINDER90)
Predictor-Corrector	Semi-PC	Full-PC

Table 7
Comparison of computing time and memory usage for MTR depletion.

Number of burnup regions	Execution time (core-hours)			Memory per CPU (MB)		
	MCS	MCNP6	Ratio	MCS	MCNP6	Ratio
4	552	6637	12.0	952	4092	4.3
18	552	6982	12.6	956	4122	4.8

5. Dependency of k-eff in depletion to the fuel segmentation

The influence of the axial and radial modeling of the burnup distribution in the fuel plates of the MTR on the k-eff of the MTR in depletion is investigated. The MTR core consists of 18 fuel assemblies made each of 21 fuel meats of height 64 cm, thickness 0.051 cm and width 6.21 cm in width. Segmentation of the fuel plates along the height and the width is considered in this section.

All the calculations are conducted in the same conditions as in the previous verification section, especially, room-temperature cross sections are employed. Other parameters that may have an impact on the k-eff of the MTR in depletion but that are not investigated are the irradiation history of the MTR, and the temperature of the coolant and of the fuel meats at 5 MW thermal power.

5.1. Cell-wise depletion with axial fuel segmentation

Four depletion simulations with 1 radial mesh and 1, 7, 10 and 20 axial meshes per fuel meat are conducted with MCS to observe the effect on the k-eff and cycle length of the MTR. The corresponding numbers of depletion cells for each simulation are respectively 378; 2,646; 3,780; and 7,560 depletion cells. The evolution of the k-eff as a function of time is shown in the left-hand side of Fig. 13 and the differences between the 20-axial-mesh calculation and the other calculations with the error bars plotted at one standard deviations are shown in the right-hand side of Fig. 13. The results for 7, 10 and 20 axial zones are essentially the same within 100 pcm whereas the results for 1 axial zone per fuel plate drift apart with increasing burnup. The calculations therefore support the use of at least 7 axial zones per fuel meat for precise depletion simulation of the MTR. Further depletion calculations in this section will use at least 10 axial zones per fuel meat out of conservativeness.

The calculated cycle length of the MTR is 82.7 EFPDs when using 20 axial meshes and 91.9 EFPDs when using one axial meshes. This difference is due to the fact that the 20-axial-mesh calculation models the axial gradient of burnup and is therefore more precise

Table 8
Comparison of material-wise depletion in MCS and MCNP6 for 100 EFPDs.

Steps	EFPD (Days)	Burn up (GWd/MTU)	k-eff ± uncertainty (pcm)		Diff* ± 1σ (pcm)
			MCS	MCNP6	
0	0	0.000	1.08204 ± 25	1.08232 ± 23	−28 ± 34
1	0.01	0.001	1.08207 ± 24	1.08162 ± 25	45 ± 35
2	0.02	0.003	1.08170 ± 26	1.08142 ± 28	28 ± 38
3	0.03	0.004	1.08158 ± 29	1.08181 ± 25	−23 ± 39
4	0.04	0.005	1.08184 ± 25	1.08071 ± 25	113 ± 35
5	0.08	0.011	1.07969 ± 26	1.07893 ± 26	76 ± 37
6	0.12	0.016	1.07792 ± 25	1.07774 ± 25	18 ± 35
7	0.185	0.025	1.07498 ± 29	1.07469 ± 25	29 ± 38
8	0.25	0.033	1.07152 ± 28	1.07102 ± 23	50 ± 36
9	0.625	0.083	1.05747 ± 27	1.05723 ± 26	24 ± 37
10	1	0.133	1.05112 ± 27	1.05101 ± 25	11 ± 36
11	1.5	0.199	1.04787 ± 29	1.04790 ± 25	−3 ± 38
12	2	0.266	1.04674 ± 28	1.04669 ± 24	5 ± 37
13	3	0.399	1.04557 ± 25	1.04531 ± 23	26 ± 34
14	4	0.531	1.04436 ± 24	1.04423 ± 26	13 ± 35
15	6	0.797	1.04193 ± 25	1.04225 ± 24	−32 ± 35
16	8	1.063	1.04054 ± 27	1.04103 ± 28	−49 ± 39
17	10	1.328	1.03912 ± 25	1.03866 ± 26	46 ± 36
18	12	1.594	1.03718 ± 28	1.03714 ± 24	4 ± 37
19	14	1.860	1.03645 ± 24	1.03637 ± 26	8 ± 35
20	16	2.125	1.03489 ± 25	1.03471 ± 25	18 ± 36
21	20.5	2.723	1.03252 ± 26	1.03251 ± 26	1 ± 37
22	25	3.321	1.03069 ± 24	1.03006 ± 24	63 ± 34
23	32.5	4.317	1.02695 ± 25	1.02719 ± 24	−24 ± 34
24	40	5.313	1.02430 ± 25	1.02385 ± 23	45 ± 34
25	47.5	6.309	1.02101 ± 27	1.02072 ± 24	29 ± 36
26	55	7.305	1.01691 ± 25	1.01727 ± 27	−36 ± 37
27	62.5	8.301	1.01400 ± 25	1.01376 ± 24	24 ± 34
28	70	9.298	1.01038 ± 28	1.01019 ± 24	19 ± 37
29	77.5	10.290	1.00732 ± 27	1.00722 ± 25	10 ± 37
30	85	11.290	1.00404 ± 28	1.00377 ± 26	27 ± 38
31	92.5	12.290	1.00078 ± 26	1.00043 ± 24	35 ± 35
32	100	13.280	0.99690 ± 26	0.99633 ± 20	57 ± 33

$Diff^* = 10^5 \times (k_{MCS} - k_{MCNP6})$

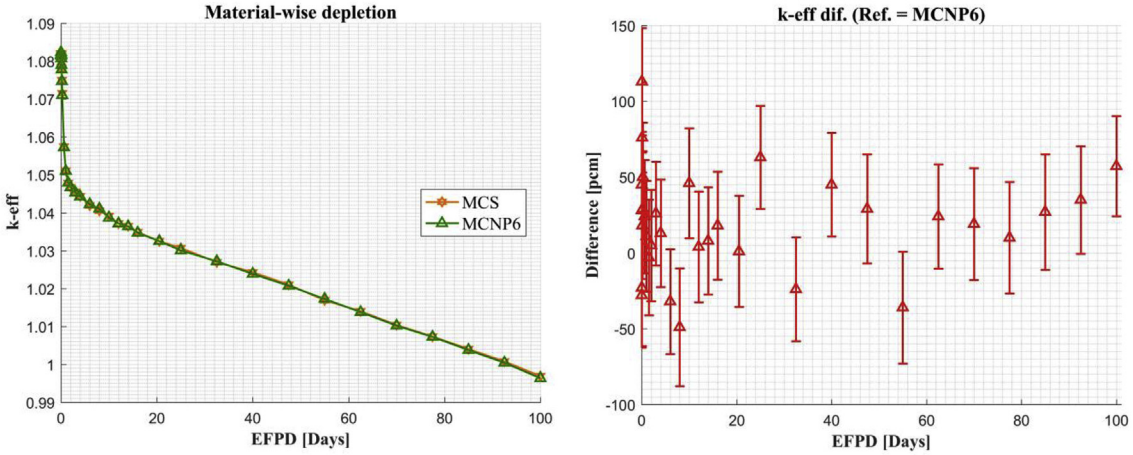

Fig. 11. Evolution of k-eff over depletion time for the MTR material-wise depletion.

Table 9
Comparison of assembly-wise depletion in MCS and MCNP6 for 100 EFPDs.

Steps	EFPD (Days)	Burn up (GWd/MTU)	k-eff ± uncertainty (pcm)		Diff* ± 1σ (pcm)
			MCS	MCNP6	
0	0	0.000	1.08204 ± 25	1.08133 ± 25	71 ± 36
1	0.01	0.001	1.08221 ± 28	1.08127 ± 27	94 ± 39
2	0.02	0.003	1.08242 ± 29	1.08133 ± 25	109 ± 39
3	0.03	0.004	1.08124 ± 25	1.08146 ± 25	−22 ± 35
4	0.04	0.005	1.08120 ± 26	1.08060 ± 25	60 ± 36
5	0.08	0.011	1.07917 ± 29	1.07956 ± 24	−39 ± 37
6	0.12	0.016	1.07775 ± 29	1.07802 ± 26	−27 ± 39
7	0.185	0.025	1.07432 ± 26	1.07476 ± 25	−44 ± 36
8	0.25	0.033	1.07154 ± 26	1.07077 ± 26	77 ± 37
9	0.625	0.083	1.05751 ± 27	1.05700 ± 26	51 ± 37
10	1	0.133	1.05115 ± 25	1.05104 ± 26	11 ± 36
11	1.5	0.199	1.04820 ± 26	1.04791 ± 25	29 ± 36
12	2	0.266	1.04638 ± 25	1.04654 ± 26	−16 ± 36
13	3	0.399	1.04574 ± 26	1.04499 ± 24	75 ± 35
14	4	0.531	1.04451 ± 24	1.04376 ± 23	75 ± 33
15	6	0.797	1.04236 ± 26	1.04249 ± 25	−13 ± 36
16	8	1.063	1.04051 ± 26	1.04058 ± 26	−7 ± 36
17	10	1.328	1.03861 ± 26	1.03860 ± 27	1 ± 37
18	12	1.594	1.03716 ± 26	1.03725 ± 23	−9 ± 35
19	14	1.860	1.03641 ± 26	1.03589 ± 24	52 ± 35
20	16	2.125	1.03464 ± 28	1.03479 ± 23	−15 ± 36
21	20.5	2.723	1.03282 ± 25	1.03240 ± 24	42 ± 35
22	25	3.321	1.03031 ± 25	1.03033 ± 25	−2 ± 35
23	32.5	4.317	1.02707 ± 25	1.02638 ± 24	69 ± 35
24	40	5.313	1.02419 ± 26	1.02302 ± 25	117 ± 36
25	47.5	6.309	1.02074 ± 26	1.02031 ± 25	43 ± 36
26	55	7.305	1.01725 ± 25	1.01723 ± 23	2 ± 34
27	62.5	8.301	1.01374 ± 24	1.01376 ± 25	−2 ± 35
28	70	9.298	1.01081 ± 26	1.00992 ± 24	89 ± 36
29	77.5	10.290	1.00771 ± 23	1.00683 ± 24	88 ± 33
30	85	11.290	1.00383 ± 24	1.00386 ± 23	−3 ± 33
31	92.5	12.290	1.00050 ± 23	0.99997 ± 25	53 ± 34
32	100	13.280	0.99748 ± 25	0.99666 ± 25	82 ± 35

$Diff^* = 10^5 \times (k_{MCS} - k_{MCNP6})$

than the 1-axial-mesh calculation that depletes the fuel uniformly in the axial direction. This difference in modeling is illustrated in Fig. 14 which corresponds to the axial burnup distribution at 47.5 EFPD (step 25) of the central fuel plate number 11 in assembly FA04. For this fuel plate, the axial burnup distribution of the 1-axial-mesh depletion is a flat line whereas the 20-axial-mesh depletion shows low burnup regions at the bottom and top of the assembly and a high burnup region close to the axial core mid-plane.

5.2. Cell-wise depletion with radial fuel segmentation

Three depletion simulations with 10 axial meshes and 1, 3 and 10 radial meshes per fuel meat are conducted with MCS to observe the effect on the k-eff and cycle length of the MTR. The corresponding numbers of depletion cells for each simulation are respectively 3,780; 11,340; and 37,800 depletion cells. The evolution of the k-eff as a function of time is shown in the left-hand side of Fig. 15 and the differences between the 10-radial-mesh calculation and the other

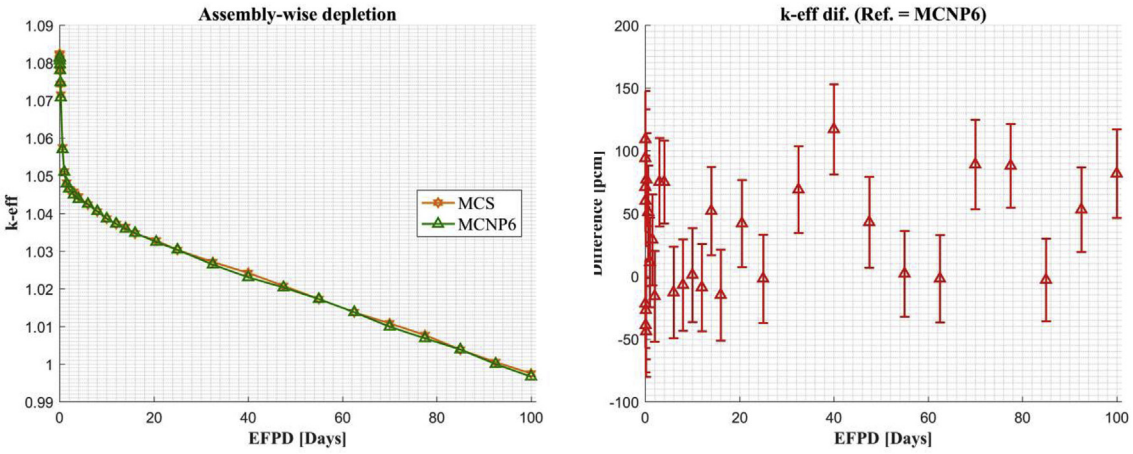

Fig. 12. Evolution of k-eff over depletion time for the MTR assembly-wise depletion.

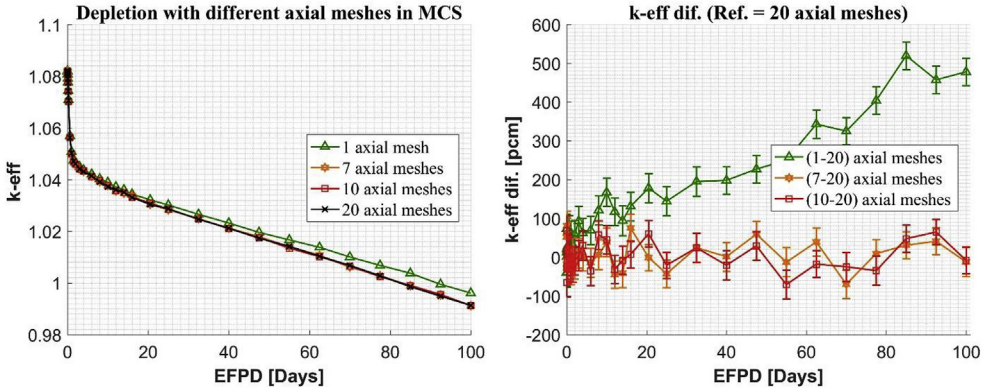

Fig. 13. Cell-wise depletion of the MTR with different axial meshes.

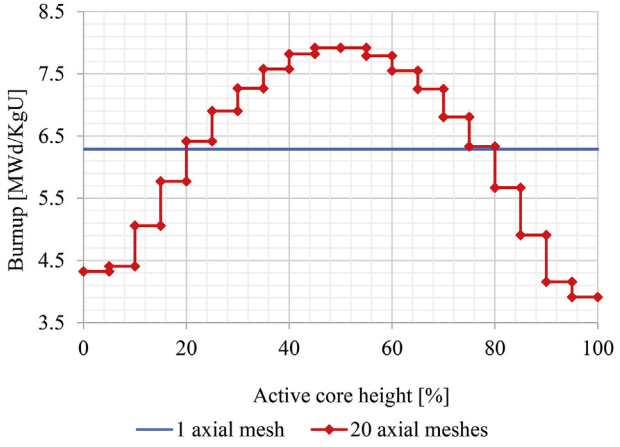

Fig. 14. Axial burnup distribution at 47.5 EFPDs for the central fuel plate number 11 of assembly F04 with 1 and 20 axial meshes.

calculations with the error bars plotted at one standard deviations are shown in the right-hand side of Fig. 15. The results for 1, 3 and 10 radial meshes per fuel plate are essentially the same within 100 pcm, thus underlying that radial segmentation of the fuel does not bring more precise depletion results. The cycle length predicted by the reference depletion calculation (10 radial meshes and 10 axial meshes per fuel meat) amounts to 82.3 EFPDs.

5.3. Material-wise/assembly-wise depletion with axial fuel segmentation

Depletion calculations with much fewer depletion cells, but still precise enough k-eff results, are tested with MCS. Two calculations are tested: material-wise depletion with 10 axial meshes per fuel meat (4 fuel materials x 10 axial meshes = 40 depletion cells) and assembly-wise depletion with 10 axial meshes per fuel meat (18 assemblies x 10 axial meshes = 180 depletion cells), and compared against the plate-wise depletion with 10 meshes per fuel meat (18 assemblies x 21 fuel meats x 10 axial meshes = 3780 depletion cells). The evolution of k-eff as a function of time in shown in the left-hand side of Fig. 16 whereas the difference between the plate-wise depletion and the other calculations with error bars plotted at one standard deviation are shown in the right-hand side of Fig. 16. A maximum difference of 140 pcm is observed between the 40-/180-depletion-cell calculations and the 3780-depletion-cell calculation. A similar cycle length of 83–85 EFPDs is observed for the three depletion simulations. It is therefore possible to obtain k-eff results within 140 pcm of a reference depletion calculation by only modeling in detail the axial distribution of burnup in the MTR core.

The execution time and memory usage of MCS when going from a 40-depletion-cell calculation to a 3780-depletion-cell calculation are not significantly different. The execution time of 3780-depletion-cell calculation in MCS is 559 core-hours with a memory use of 1061 MB. This representsa overhead only compared to simulation results of Table 7. The 40- and 180-depletion-cell

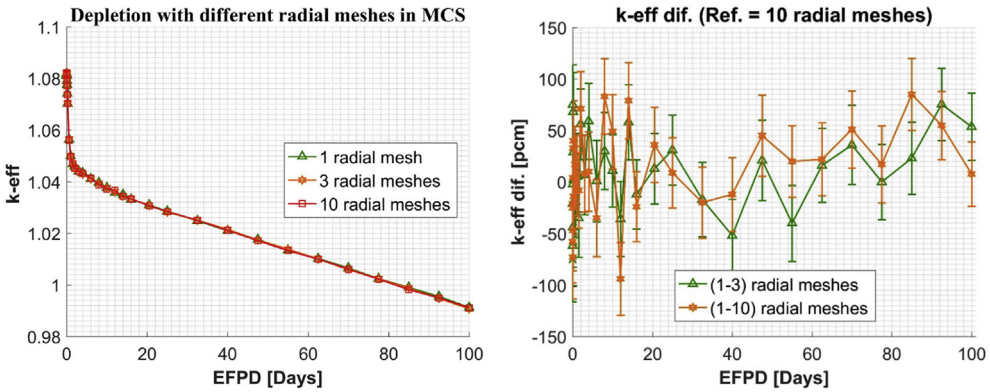

Fig. 15. MTR cell-wise depletion with different radial meshes.

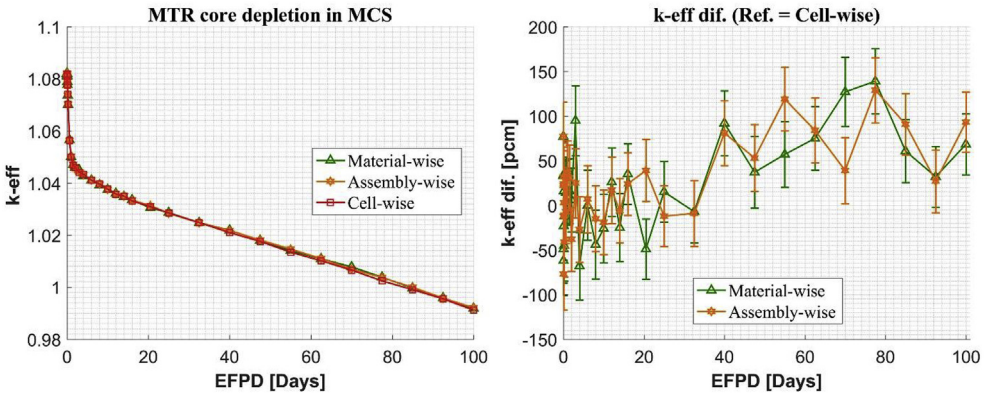

Fig. 16. 10 axially sub-divided depletion of MTR model.

Table 10
Estimated computing time and memory used in MCNP6 depletion calculations.

	Simulated		Interpolated		Factor	
Number of burnup regions	4	18	40	180	Material wise	Assembly wise
Execution time (core-hours)	6637	6982	7524	10,974	1.1	1.0
Memory per CPU (MB)	4092	4122	4169	4469	1.6	1.1

calculations are not performed with MCNP6 and the corresponding computing time and memory are estimated instead by interpolation of the results from Table 7 in terms of the number of depletion cells (from 4 to 40 and 18 to 180 depletion cells) and shown in Table 10. MCS shows very little overhead compared to MCNP in terms of execution time and memory, even for problems with thousand more depletion cells.

6. Conclusions and perspectives

A complex material-testing reactor depletion problem with 37,800 depletion cells (18 assemblies, 21 fuel plates per assemblies, 10 axial meshes and 10 radial meshes per fuel plate) is solved with the Monte Carlo code MCS on a cluster with 40 CPUs with about 1 GB memory use per CPU and in less than 600 core-hours. This performance is achieved thanks to a combination of good algorithms implemented in MCS: parallel fission bank algorithm for reduced communication of fission sources and enhanced CPU-scalability during the transport steps (criticality calculations); use of CRAM solver with a smart memory allocation scheme for the depletion-related variables, enabling to reduce the memory use per CPU as the number of CPUs increase; an hash indexing algorithm that allows to retrieve the index of tally bins in negligible time, enabling small tally overhead even when handling millions of tally; and a semi predictor-corrector depletion scheme which represents a good trade-off between an accurate but time-consuming full predictor-corrector scheme and a less accurate but faster simple predictor scheme.

The suitability of MCS for the criticality and depletion analysis is confirmed through the comparisons against MCNP6 of control rod worth, neutron flux, kinetic parameters, and power peaking factor at beginning of cycle and of k-eff in depletion for two simple MTR depletion problems, which show good agreements within the statistical uncertainties. MCS depletion capability is verified against MCNP6 for the material-wise (4-depletion-cell) and assembly-wise (18-depletion-cell). MCS show good accuracy of k-eff results within 3 statistical uncertainties and highlights the small overhead in execution time and memory usage compared to MCNP6. The study shows the user-friendliness of MCS code when modeling the complex MTR geometry with 37,800 depletion cells. MCS demonstrates the necessity to determine the minimum requirement for the spatial

segmentation of the fuel plates in MTR with at least of 7 axial meshes to obtain the same precision of accuracy compared to reference (reference calculation with 10 radial meshes and 10 axial meshes per fuel plate). MCS depletion result with 7560 depletion-cells (20 axial meshes) is 10 EFPDs shorter than the cycle length from depletion result with 378 depletion-cells (1 axial meshes). MCS depletion with 37,800 depletion-cell (10 axial meshes, and 10 radial meshes) shows similar cycle length to the 3780 depletion-cell (10 axial meshes, and 1 radial meshes) due to very thin thickness of the fuel plate. MCS depletion results from 4 depletion cell (material-wise) to 37,800 depletion cell calculation shows no significant difference in the execution time and memory usage compared to MCNP6. When dealing with depletion problems, it is showcased that MCS can overcome the code issues of MCNP in terms of computing time, memory use requirements and ability to generate results with high enough precision and accuracy.

The next step for the depletion capability of MCS is the study of the propagation of the statistical uncertainties of tallied reaction rates in the Bateman equations and the resulting uncertainties on the material compositions and flux in the reactor. It is also envisioned to develop MCS models to conduct the neutronic and depletion analysis of other material-testing reactors such as the Kartini TRIGA Mark II research reactor in Indonesia (Training, Research, Isotope, General Atomic) [43] and the HANARO reactor in South Korea (High-Flux Advanced Neutron Application Reactor) [44].

Declaration of competing interest

The authors declare that they have no known competing financial interests or personal relationships that could have appeared to influence the work reported in this paper.

Acknowledgements

This work was supported by the National Research Foundation of Korea (NRF) grant funded by the Korea government (MSIT). (No. NRF-2019M2D2A1A03058371).

References

[1] S.A. El-mongy, Overview of Research Reactors (RR) Worldwide and Their Applications, 2018.
[2] Saclay CEA, OSIRIS Nuclear Reactors and Services Department, 2008.
[3] C. Gonnier, J. Estrade, G. Bignan, et al., Experimental devices in Jules Horowitz reactor and first orientations for the experimental programs, in: Proceedings of IGORR 18th Meeting, Sydney, Australia, December, 2017.
[4] C.J. Stanley, F.M. Marshall, Advanced test reactor— A national scientific user facility, in: Proceedings of ICONE 16th Conference, Orlando, Florida, USA, May 11–15, 2008, https://doi.org/10.1115/icone16-48426.
[5] N. Xoubi, Jordan Research and Training Reactor (JRTR) Utilization Facilities, 2010. IAEA-TM-38728.
[6] E. Privas, C. Bouret, S. Nicolas, et al., Monte-carlo coupled depletion codes efficiency for research reactor design, in: Proceedings of IGORR 18th Meeting, Sydney, Australia, December, 2017.
[7] A. Péron, F. Malouch, C.M. Diop, Improvement of nuclear heating evaluation inside the core of the OSIRIS material testing reactor, in: Proceedings of EPJ Web of Conferences, vol. 106, 2016, https://doi.org/10.1051/epjconf/201610605006, 05006.
[8] D. Parrat, G. Bignan, B. Maugard, et al., The future Jules Horowitz material testing reactor: an opportunity for developing international collaborations on a major European irradiation infrastructure, in: Proceedings of International Conference on WWER Fuel Performance, Modelling and Experimental Support, Vama, Bulgaria, September 26– October 3, 2015.
[9] F. Jeury, J. Politello, C. D'Aletto, et al., HORUS3D/N neutron calculation tool, a deterministic scheme dedicated to JHR design and safety studies, Nucl. Sci. Eng. 189 (2018) 188–198, https://doi.org/10.1080/00295639.2017.1381505.
[10] W. Haeck, B. Cochet, L. Aguiar, Monte Carlo depletion calculations using VESTA 2.1 new features and perspectives, in: Proceedings of PHYSOR Conference, Knoxville, Tennessee, USA, April 15–20, 2012.
[11] D.B. Pelowitz, J.T. Goorley, M.R. James, et al., MCNP6 USER'S MANUAL Version 1.0, LA-CP-13-00634, Rev. 0, 2013.
[12] H. Lee, W. Kim, P. Zhang, et al., MCS – a Monte Carlo particle transport code for large-scale power reactor analysis, Ann. Nucl. Energy (2019). https://doi.org/10.1016/j.anucene.2019.107276.
[13] J. Yu, H. Lee, M. Lemaire, et al., MCS based neutronics/thermal-hydraulics/fuel-performance coupling with CTF and FRAPCON, Comput. Phys. Commun. 238 (2019) 1–18, https://doi.org/10.1016/j.cpc.2019.01.001.
[14] M.K. Jaradat, V. Radulović, C.J. Park, et al., Verification of MCNP6 model of the Jordan Research and Training Reactor (JRTR) for calculations of neutronic parameters, Ann. Nucl. Energy 96 (2016) 96–103, https://doi.org/10.1016/j.anucene.2016.06.003.
[15] K.O. Kim, B.J. Jun, B. Lee, et al., Neutronics experiment results in commissioning stage B of JRTR, in: Proceedings of RRFM Conference, Munich, Germany, March 11-15, 2018.
[16] J. Jang, W. Kim, S. Jeong, et al., Validation of UNIST Monte Carlo code MCS for criticality safety analysis of PWR spent fuel pool and storage cask, Ann. Nucl. Energy 114 (2018) 495–509, https://doi.org/10.1016/j.anucene.2017.12.054.
[17] J. Yu, H. Lee, H. Kim, et al., Preliminary coupling of the Thermal/Hydraulic solvers in the Monte Carlo code MCS for practical LWR analysis, Ann. Nucl. Energy 118 (2018) 317–335, https://doi.org/10.1016/j.anucene.2018.03.043.
[18] H. Lee, C. Kong, D. Lee, Status of Monte Carlo code development at UNIST, in: Proceedings of PHYSOR Conference, the Westin Miyako, Kyoto, Japan, September 28– October 3, 2014 ([USB]).
[19] T.D.C. Nguyen, H. Lee, S. Choi, et al., Validation of UNIST Monte Carlo code MCS using VERA progression problems, Nucl. Eng. Tech. (2019), https://doi.org/10.1016/j.net.2019.10.023.
[20] B. Ebiwonjumi, H. Lee, J. Choe, et al., MCS analysis of Westinghouse 3-loop PWR multi-cycle operation, in: Proceedings of KNS Autumn Meeting, Yeosu, Korea, October 25–26, 2018 ([USB]).
[21] V. Dos, H. Lee, J. Choe, et al., Validation of Monte Carlo MCS code for OPR -1000 operation, in: Proceedings of NURER Conference, Ramada Plaza Jeju, Korea, September 30– October 3, 2018 ([USB]).
[22] H. Lee, E. Jeong, H. Lee, et al., Verification of MCS VHTR modeling capability, in: Proceedings of RPHA17 Conference, Chengdu, China, August 24–25, 2017 ([USB]).
[23] T.D.C. Nguyen, H. Lee, et al., LPPT analysis of APR1400 reactor core by UNIST Monte Carlo code MCS, in: Proceedings of RPHA17 Conference, Chengdu, China, August 24–25, 2017 ([USB]).
[24] T.D.C. Nguyen, J. Choe, B. Ebiwonjumi, et al., Core design of long-cycle small modular lead-cooled fast reactor, Int. J. Energy Res. 43 (2019) 254–273, https://doi.org/10.1002/er.4258.
[25] P. Zhang, H. Lee, D. Lee, On the transfer matrix of the modified power method, Comput. Phys. Commun. 222 (2018) 102–112, https://doi.org/10.1016/j.cpc.2017.09.022.
[26] H. Lee, S. Choi, D. Lee, A hybrid Monte Carlo/Method-of-Characteristics method for efficient neutron transport analysis, Nucl. Sci. Eng. 180 (2015) 69–85, https://doi.org/10.13182/NSE13-102.
[27] P.K. Romano, B. Forget, Parallel fission bank algorithms in Monte Carlo criticality calculations, Nucl. Sci. Eng. 170 (2017) 125–135, https://doi.org/10.13182/NSE10-98.
[28] M. Pusa, J. Leppänen, Computing the matrix exponential in burnup calculations, Nucl. Sci. Eng. 164 (2017) 140–150, https://doi.org/10.13182/NSE09-14.
[29] A.E. Isotalo, P.A. Aarnio, Comparison of depletion algorithms for large systems of nuclides, Ann. Nucl. Energy 38 (2011) 261–268, https://doi.org/10.1016/j.anucene.2010.10.019.
[30] J. Park, A. Khassenov, W. Kim, et al., Comparative analysis of VERA depletion benchmark through consistent code-to-code comparison, Ann. Nucl. Energy 124 (2019) 385–398, https://doi.org/10.1016/j.anucene.2018.10.024.
[31] W. Kim, H. Lee, S. Choi, et al., Hybrid depletion method for the light water reactor analysis wonkyeong, in: Proceeding of M&C 2017 Conference, Jeju, Korea, April 16–20, 2017 ([USB]).
[32] H. Lee, Development of a New Monte Carlo Code for High-Fidelity Power Reactor Analysis Thesis (Doctoral), Ulsan National Institute of Science and Technology, 2019 ([USB]).
[33] B.T. Mervin, Monte Carlo and Depletion Reactor Analysis for High-Performance Computing Applications, Doctoral Dissertation University of Tennessee - Knoxville, 2013. https://trace.tennessee.edu/utk_graddiss/2601.
[34] V. Dos, H. Lee, Y. Jo, et al., Verification of MCS Monte Carlo code for the JRTR research reactor, in: Proceedings of the PHYSOR Conference, Cancun: American Nuclear Society, Apr 22–26, 2018 ([USB]).
[35] K.O. Kim, B.J. Jun, B. Lee, et al., Comparison of first criticality prediction and experiment of the Jordan research and training reactor (JRTR), Nucl. Eng. Tech. (2019) 6–10, https://doi.org/10.1016/j.net.2019.06.027.
[36] I.F. Farouki, Full-core burn-up calculations using MCNP6 code for the Jordan research and training reactor, in: Proceeding of Research Reactor Fuel Management Conference, Amman, Jordan, March, 2019.
[37] A.H. Fadaei, S. Setayeshi, Control rod worth calculation for VVER-1000 nuclear reactor using WIMS and CITATION codes, Prog. Nucl. Energy 51 (2009) 184–191, https://doi.org/10.1016/j.pnucene.2008.03.003.
[38] Y. Qiu, Z. Wang, K. Li, et al., Calculation of adjoint-weighted kinetic parameters with the reactor Monte Carlo code RMC, Prog. Nucl. Energy 101 (2017) 424–434, https://doi.org/10.1016/j.pnucene.2017.03.023.
[39] M.H. Rabir, M.R.M. Zin, M.D, et al., Neutron flux and power in RTP core-15, in:

Proceeding of AIP Conference, vol. 1704, 2016, https://doi.org/10.1063/1.4940114, 050018-1–050018-11.
[40] M.L. Fensin, M.R. James, J.S. Hendricks, et al., The new MCNP6 depletion capability, in: Proceedings of ICAPP Conference, Chicago, USA, June 24–28, 2012.
[41] I.J. Bratton, Modeling and Validation of the Fuel Depletion and Burnup of the OSU Research Reactor Using MCNPX/CINDER'90, Thesis (Master), The Ohio State University, 2012.
[42] J.S. Hendricks, G.W. Mckinney, M.L. Fensin, et al., MCNPX 2.6.0 Extensions, LA-UR-08-2216, April 11, 2008.
[43] U.S. Hidayat, A. Agung, M. Lemaire, et al., MCS cycle depletion analysis and validation of excess reactivity and shutdown margin for the Kartini triga Mark II research reactor, in: Proceedings of ICAPP Conference, Juan-Les-Pins, France, May 12–15, 2019.
[44] K.N. Choo, M.S. Cho, S.W. Yang, et al., Contribution of Hanaro irradiation technologies to national nuclear R&D, Nucl. Eng. Technol. 46 (2014) 501–512, https://doi.org/10.5516/NET.07.2014.006.